AIP Advances

Revealing the quasiparticle electronic and excitonic nature in cubic, tetragonal, and hexagonal phases of $FAPbI_3$

Cite as: AIP Advances **12**, 025330 (2022); https://doi.org/10.1063/5.0076738
Submitted: 29 October 2021 • Accepted: 01 February 2022 • Published Online: 23 February 2022

Zeeshan Muhammad, Peitao Liu, Rashid Ahmad, et al.

Revealing the quasiparticle electronic and excitonic nature in cubic, tetragonal, and hexagonal phases of $FAPbI_3$

Cite as: AIP Advances 12, 025330 (2022); doi: 10.1063/5.0076738
Submitted: 29 October 2021 • Accepted: 1 February 2022 •
Published Online: 23 February 2022

Zeeshan Muhammad,[1,2,a)] Peitao Liu,[3,4] Rashid Ahmad,[1,5] Saeid Jalali-Asadabadi,[6] Cesare Franchini,[3,7] and Iftikhar Ahmad[1,8]

AFFILIATIONS

[1] Center for Computational Material Science, University of Malakand, Chakdara, Pakistan
[2] Department of Physics, University of Malakand, Chakdara, Pakistan
[3] University of Vienna, Faculty of Physics and Center for Computational Materials Science, Sensengasse 8, A-1090 Vienna, Austria
[4] Shenyang National Laboratory for Materials Science, Institute of Metal Research, Chinese Academy of Sciences, Shenyang 110016, People's Republic of China
[5] University of Malakand, Chakdara, Pakistan
[6] Department of Physics, Faculty of Physics, University of Isfahan (UI), Hezar Jerib Avenue, Isfahan 81746-73441, Iran
[7] Dipartimento di Fisica e Astronomia, Università di Bologna, 40127 Bologna, Italy
[8] Gomal University, Dera Ismail Khan, Pakistan

[a)] **Author to whom correspondence should be addressed:** zeeshan_muhammad@uom.edu.pk

ABSTRACT

The development of three-dimensional (3D) hybrid organic–inorganic perovskites has sparked much interest because of their rich light-harvesting capabilities in solar cells. However, the understanding of the electronic and optical properties, particularly the excitonic shifts upon structural phase transition with temperature in these materials, is not fully clear. Here, we report the accurate description of electronic and optical properties of mostly studied $FAPbI_3$ across the cubic–tetragonal–hexagonal phases, using the relativistic GW method and Bethe–Salpeter Equation (BSE), including the spin–orbit coupling effects. Our GW calculations reveal that the bandgap values vary from 1.47 to 3.54 eV from the room temperature cubic phase to the low temperature hexagonal phase. Our optical analysis shows that excitonic peaks are blue-shifted, and exciton binding energies estimated by the model BSE approach increase from 74 to 567 meV going from the cubic to hexagonal phases. Our results may have important impacts on the practical uptake of hybrid perovskite based solar cells under different climatic conditions.

INTRODUCTION

Hybrid organic–inorganic perovskite (HOIP), having general formula ABX_3 (where A is the organic cation, B is the smaller divalent cation, and X is the monovalent metal halide), is the most promising class of semiconducting photovoltaic materials, which has gained a leading role in the field of solar cell technologies because of its low-cost and high-power conversion efficiency up to 27.0% for perovskite/Si based tandem solar cells.[1] Some of the key characteristics of these materials that make them exceptional are their tunable optimal bandgap for appropriate sunlight absorption,[2–6] longer carrier lifetimes,[7,8] high charge carrier mobility,[9–11] long charge carrier diffusion length,[11–13] high rotational entropy of organic cation,[14] and weak excitonic binding energies.[15–22] Among all HOIPs, methylammonium lead iodide ($CH_3NH_3PbI_3$ or $MAPbI_3$) and formamidinium lead iodide

$[CH(NH_2)_2PbI_3$ or $FAPbI_3]$ have been foremost considered by researchers so far. Due to lower bandgap, better stability, and enhanced carrier transport properties, $FAPbI_3$ represents one of the best candidates for efficient solar cell devices.

The power-conversion efficiency of a solar cell material varies with its electrical and optical properties. These properties depend on various physical parameters, such as lattice parameters, bandgaps, and absorption. In addition, the structural transition upon change in temperature plays an important role in the performance of the solar cell. Due to the large contribution of electron–hole (e–h) interactions in the excited systems, the interplay of excitonic effects cannot be ignored.[15–22] According to literature, the interaction of the e–h pair can be influenced by three basic factors. First, according to the ferroelectric domain theory,[23–27] the alignment of organic cations causes generation of nanoscale ferroelectric domains that make spatial separation of the photoexcited electron and hole pairs and thereby degrading their process of recombination. Second, from the Rashba–Dresselhaus splitting effect,[28–31] the spin and orbital motion of the inorganic atoms interacts with the electric field produced by the organic cations, thus resulting in the splitting of electronic band structure for different spins, and leads to an effective indirect bandgap and enhanced carrier lifetime. Third, the formation of large polarons[32] due to reorientation of organic cations causes charge separation in response to optical excitation and thus reduces the quasiparticle energy of electron and hole.[7,16,31,33] Experimentally, it has also been found that ionic screening is affected by temperature.[16–19,22] Previously, the photoluminescence (PL) studies of $FAPbI_3$ in the temperature range of 400–100 K showed degradation in PL spectra going from the cubic-to-hexagonal phase.[14] However, in a few articles, it has been shown that screening effects do not seem to be directly influenced by the change in temperature.[20,21] In another study, kinetic trapping is found to influence the electronic and optical excitonic properties during the phase transition of $FAPbI_3$.[34] Therefore, to address such controversial problem, it is requisite to study excitonic properties on microscopic correlations between the ionic screening and the prolonged charge carrier lifetime from an *ab initio* calculation point of view.

In this work, we study the detailed changes in quasi-particle electronic energies and optical excitonic behavior due to the structural transition from the cubic to tetragonal to hexagonal phase for the $FAPbI_3$ system. We employ density functional theory (DFT) to obtain ground-state structures and many-electron GW method to calculate the quasi-particle energies and bandgaps (E_g).[16,35–39] The presence of heavy elements, such as Pb, requires to account for the relativistic effects, including spin–orbit coupling (SOC). At the end, to evaluate exciton binding energies (E_b) and obtain accurate description of the optical spectra, the e–h interactions have to be accounted for by solving the Bethe–Salpeter equation combined with GW calculations.[40–42] Computing the fundamental material properties as a function of the structural phase is exclusively requisite for the device design, since a significant variation in the material's electronic and optical characteristics is typically linked with a temperature-dependent structural phase transition. Such transitional behaviors are not easy to accommodate in a photovoltaic device while keeping efficient carrier extraction with carrier-selective metallization, as they must be precisely compatible with the light-absorber under any climatic environment.

COMPUTATIONAL DETAILS

Starting from the $FAPbI_3$ experimental geometry of the cubic phase (α) at 298 K,[43,44] tetragonal phase (β) at 220 K,[14] and hexagonal phase (δ) at 15 K,[34] we performed DFT calculations using the Vienna *ab initio* simulation package (VASP)[45,46] with the projector augmented wave (PAW) pseudopotentials.[47] For the exchange correlation functional, the generalized gradient approximation (GGA) parameterized by Perdew–Burke–Ernzerhof (PBE) was used.[48,49] A energy cutoff of 600 eV and Γ-centered 6 × 6 × 6 k-point grids were used. The valence electron configurations included in the calculations are $5d^{10}6s^26p^2$ for Pb, $5s^25p^5$ for I, $2s^22p^3$ for N, $1s^1$ for H, and $2s^22p^2$ for C. All the structural parameters were fully relaxed with the criterion of 0.05 eV/Å on the forces exerted on each atom and an energy convergence threshold of 10^{-4} eV. To account for the van der Waals interactions, we used the rev-vdW-DF2 functional of Hamada.[50] The relativistic SOC effects were included due to the presence of heavy elements.

To obtain the accurate electronic structure, we carried out one-shot G_0W_0 calculations using a Γ-centered 4 × 4 × 4 k-point mesh for the α-phase and 3 × 3 × 4 for both the β- and δ-phases, 2100 empty bands, and a dielectric cutoff energy of 150 eV for each phase. The e–h interactions were accounted for by solving the BSE where the one-electron energies and screened interactions were from the preceding G_0W_0 calculations. For the detailed GW+BSE methodology that the VASP code follows, one may refer to Ref. 51.

Since the GW+BSE calculations are prohibitive at denser k-point grids, the exciton binding energies were calculated using the modeled BSE (mBSE)[16,51] at the DFT level in which the inverse of dielectric function is approximated by a model[52]

$$\varepsilon^{-1}(|\boldsymbol{k}+\boldsymbol{G}|) = 1 - \left(1-\varepsilon_\infty^{-1}\right)e^{-|\boldsymbol{k}+\boldsymbol{G}|^2/4\lambda^2},$$

where ε_∞, λ, and $\boldsymbol{G}$ are ion-clamped (high-frequency) dielectric constant, range–separation parameter, and plane-wave vector, respectively. The use of the mBSE allows for a denser k-point sampling, which is found to be important for the accurate estimation of exciton binding energy. The k-points grid for the α-phase was chosen to be 18 × 18 × 18 and for the β-phase and δ-phase to be 12 × 12 × 12 after careful convergence tests.

RESULTS AND DISCUSSIONS

Using DFT, we relaxed all the three structures, as shown in Fig. 1. The calculated lattice parameters, summarized in Table I, are in good agreement with the experimental data. In addition, the δ-phase is found to be energetically most stable, followed by the β- and α-phase with an energy difference of 0.23 and 0.28 eV/f.u., respectively. This thermodynamic stability of phases obtained at 0 K shows similar trends with the phase transition from the α-phase to β- and δ-phases with decreasing temperatures.[14,34,53]

Slight variations in bond lengths of Pb–I (3.18–3.24 Å) occur for different phases of $FAPbI_3$. The irregular vibrational motion of the FA molecule leads to the distortions of PbI_6 octahedra, thus resulting in the tilting of bond angles of I–Pb–I.[75] The rotational movement and polar nature of FA cation, relative to the PbI_6 framework, result in pseudo-symmetry rather than exact cubic, tetragonal, and hexagonal lattices. The fluctuations in the inorganic framework due to the motions of the organic cations are supported by the XRD

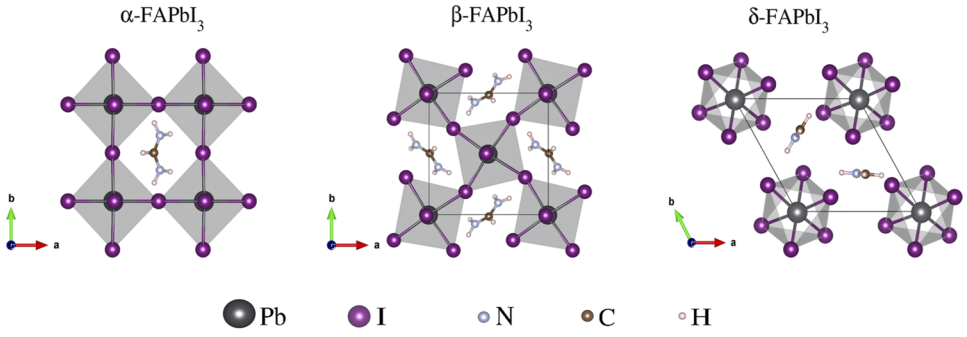

FIG. 1. Relaxed structures of $FAPbI_3$ for different phases.

TABLE I. Calculated lattice parameters for the three phases of $FAPbI_3$ using the PBE functional. The difference in ground state energies ΔE_0 with respect to the δ-phase is given for the respective phases.

Phase	Space group	Relative energy, ΔE_0 (eV/f.u.)	Calculated lattice parameters a (Å)	b (Å)	c (Å)	Experiments a (Å)	b (Å)	c (Å)
α-$FAPbI_3$ (298 K)	Pm-$3m$	0.28	6.325	6.496	6.325	6.362,[43] 6.352,[54] 6.386[34]	...	...
β-$FAPbI_3$ (220 K)	$P4/mbm$	0.23	8.900	8.925	6.344	8.926,[14] 8.923[53]	...	6.326,[14] 6.322[53]
δ-$FAPbI_3$ (15 K)	$P6_3/m$	0	8.508	8.557	7.985	8.507[34]	...	7.591[34]

analysis.[14,34,53,55] In the α-phase, the FA cation undergoes a complete disorder behavior and has a high degree of rotational freedom.[53] Such molecular orientation in the β-phase becomes anisotropic and restricted to preferential direction along with the distorted PbI_6 framework.[34,56,57] The degree of distortion in inorganic geometry becomes more pronounced in the δ-phase, leading to a complex disordered symmetry with a highly limited FA cation orientation.[34,56] In addition, Fabini *et al.* showed that the activation barrier for molecular orientation is much lower for the high temperature α-$FAPbI_3$ (21 meV) as compared to the low temperature γ-$FAPbI_3$ (84 meV).[56] Undoubtedly, such a structural transition also leads to the change in electronic and optical behavior of the material.

Table II shows the calculated bandgaps at various levels of theory. Although PBE yields a bandgap that is very close to the experimental one, this agreement is known to be fortuitous,[58] because with the inclusion of relativistic SOC effects, the bandgaps for α-, β-, and δ-$FAPbI_3$ reduce to 0.41, 0.63, and 2.32 eV, respectively, strongly underestimating the experimental bandgaps. Our findings are consistent with previous DFT+SOC calculations for MA(Pb, Sn)X_3.[16,58,59] To obtain more accurate bandgaps, we performed the G_0W_0 calculations with the inclusion of SOC effects, which yields a bandgap of 1.47 eV for α-$FAPbI_3$ and 1.71 eV for β-$FAPbI_3$, in good agreement with the experimental values.[6,15,54,60]

To reveal the bandgap variations, Fig. 2 represents the G_0W_0+SOC calculated projected densities of states (PDOS) for the three phases of $FAPbI_3$. The organic part interacts weakly with the inorganic content and does not contribute to the DOS near the Fermi level but behaves as a charge compensating center. Noticeably, the electronic states close to the bandgap region are mostly dominated by the orbital characters of Pb and I. According to the PDOSs, the valence band maximum (VBM) is mostly formed by the p-orbitals of I, fractionally mixed with the s-orbitals of Pb, whereas the conduction band minimum (CBM) is mainly dominated by the p-orbitals of Pb along with smaller portion of the p-orbitals of I. From the structural analysis, the rearrangement in the Pb–I–Pb angles increases the average Pb–I bond length along structural transition from the α-phase to β- and δ-phases, thereby reducing the orbital interactions between Pb and I atoms. This results in an increase in the fundamental bandgap from 1.47 eV (α-$FAPbI_3$) to 3.54 eV (δ-$FAPbI_3$).

TABLE II. Calculated fundamental bandgaps using different methods. Available experimental data are also given.

	Method	α-$FAPbI_3$	β-$FAPbI_3$	δ-$FAPbI_3$
Bandgap, E_g (eV)	GGA-PBE	1.43	1.63	2.70
	PBE+SOC	0.41	0.63	2.32
	G_0W_0+SOC	1.47	1.71	3.54
	Expt.	1.47,[54] 1.48[6,60]	1.52[15]	...

The band structures for each phase are presented in Fig. 3. These band structures are obtained by using the DFT+SCISSOR method such that the GW calculated bandgap is reproduced by using an appropriate SCISSOR operator. The validity of this method

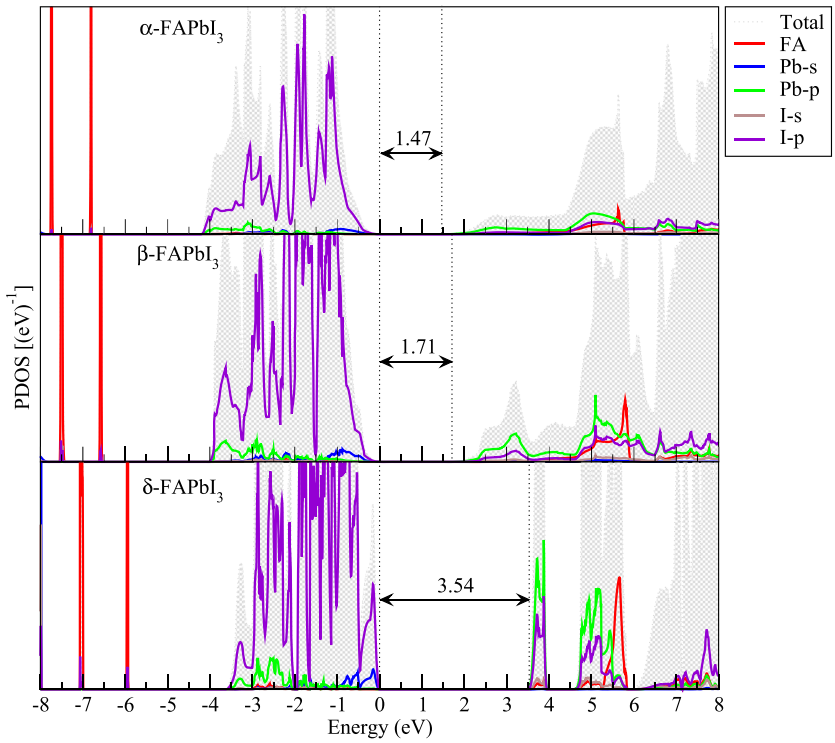

FIG. 2. G_0W_0+SOC calculated projected densities of states (PDOS) for the three phases of $FAPbI_3$.

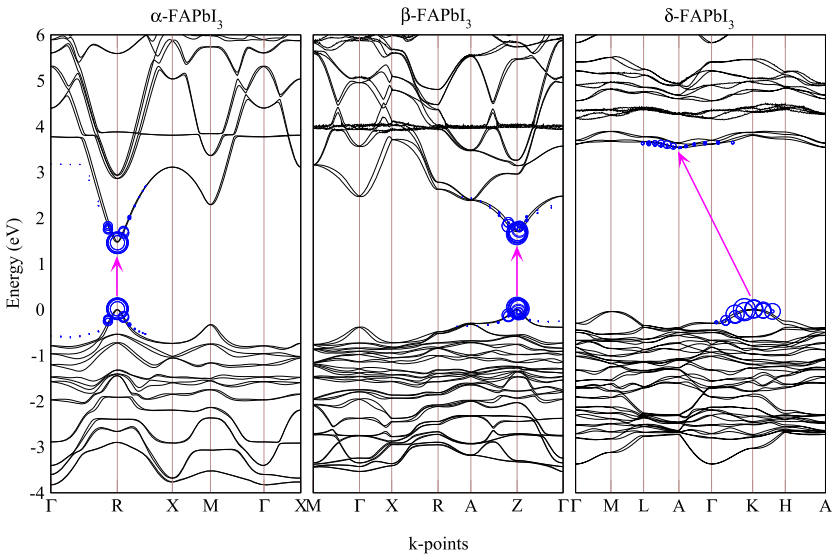

FIG. 3. Calculated band structures using the DFT+SCISSOR method for α-, β-, and δ-$FAPbI_3$. The blue circles around VBM and CBM edges represent the dominant interband transitions with the radii denoting the normalized amplitude of BSE eigenvectors.

has been justified by comparing the DFT+SCISSOR calculated band structures to the GW band structures obtained from the Wannier interpolation.[16,61] For the α- and β-phases, both VBM and CBM are located at R- and Z-points, respectively. Slight splitting in the CBM and VBM of the α- and β-phases is observed due to the Rashba–Dresselhaus effect,[28–31] while such splitting is almost negligible for the δ-phase. For both the α- and β-phases, the bandgaps are found to be direct in nature, contrary to the δ-phase that shows phonon-assisted indirect bandgap. The dispersion of both the conduction band and valence band slightly decreases moving from the α- to δ-phase, leading to the increase in bandgap values. Such dispersions can be understood by the reduced orbitals coupling near both CBM and VBM. For the analysis of the carrier transport behavior, the effective masses for the electrons $\left(m_e^*\right)$ and holes $\left(m_h^*\right)$,

TABLE III. Computed carrier effective masses for all the three phases of $FAPbI_3$. The reduced effective mass μ is calculated by using the following equation: $\mu = m_e^* \cdot m_h^* / (m_e^* + m_h^*)$.

Phase	k-path	$m_e^*(m_0)$	$m_h^*(m_0)$	$\mu(m_0)$
α-$FAPbI_3$	Γ–R and X–R	0.020	0.102	0.017
β-$FAPbI_3$	A–Z and Γ–Z	0.189	0.044	0.036
δ-$FAPbI_3$	L–A and Γ–A for CB Γ–K and H–K for VB	0.694	0.046	0.043

relative to the free electron mass m_0, are approximated by averaging along highly symmetric k-path at band edges as depicted in Table III. The dispersion equation used here is $m^* = \hbar\left[\frac{d^2E(k)}{dk^2}\right]^{-1}$, where $\hbar$ is the reduced Planck's constant, $E(k)$ is the quasiparticle energy eigenvalue, and k is the wave vector. The lower values of carrier effective masses in the α- and β-phases reveal high mobility of carriers as compared to the δ-phase. The obtained reduced carrier effective mass shows good agreement with the previously predicted data for tri-halide perovskite using the density functional theory and the k.p model.[15,58,62,63] In addition, the flattening of VBM and CBM in the δ-phase reveals enhanced phonon-assisted electron scattering with high carrier effective masses and thus has low carrier mobility in comparison to the α- and β-phases having more dispersive VBM and CBM. Our findings are consistent with previous experimental studies.[55,64]

The excitonic effects play a prominent role in understanding the relationship between optical absorption and luminescence in hybrid organic–inorganic perovskites. The optical behaviors of a material can be presented in terms of their complex real ($\mathrm{Re}[\varepsilon(\omega)]$) and imaginary ($\mathrm{Im}[\varepsilon(\omega)]$) parts of dielectric functions. The $\mathrm{Re}[\varepsilon(\omega)]$ indicates the ability of the material to permit electric field through it for storing electrical energy, while $\mathrm{Im}[\varepsilon(\omega)]$ describes absorption limits and the energy gain for the photovoltaic material.

Figure 4 shows the real ($\mathrm{Re}[\varepsilon(\omega)]$) and imaginary ($\mathrm{Im}[\varepsilon(\omega)]$) parts of the dielectric functions with the associated optical transition oscillator strengths, for all the three phases, as calculated by using the mBSE approach. Our calculated $\mathrm{Im}[\varepsilon(\omega)]$ is in overall reasonably good agreement with experiments for α-$FAPbI_3$ and δ-$FAPbI_3$. However, the computed $\mathrm{Re}[\varepsilon(\omega)]$ are highly underestimated and cross over to negative values showing metallic nature at some points for higher photon energies. In fact, at finite temperatures, the rotational dynamics of FA cation give rise to structural disorder and interfacial strain in the sample. Such effects would produce large static dielectric constant ε_0 in comparison to the simulated results at zero temperature. Further analyzing the spectrum, one observes that the whole optical spectrum shows a blue shift with the decrease in overall amplitude of oscillator strengths. As depicted in Fig. 3, the dominant excitations come from the optical transitions around the band edges at high symmetry k-point regions. The perceptive taller optical transition oscillator strengths in low energy region represent the presence of strong electron–electron and e–h interactions for the α-$FAPbI_3$ and β-$FAPbI_3$. Such excitonic feature becomes weaker for the δ-phase due to the reduced e–h recombination rate,[64] since at lower temperature, a disordered energy landscape exists due to the presence of the electric field caused by both rotating organic cations and local distortions of PbI_6 octahedra,[23] leading to smaller recombination rate. Moreover, the calculated $\mathrm{Im}[\varepsilon(\omega)]$ values show a quite consistent behavior with reduced dielectric constants due

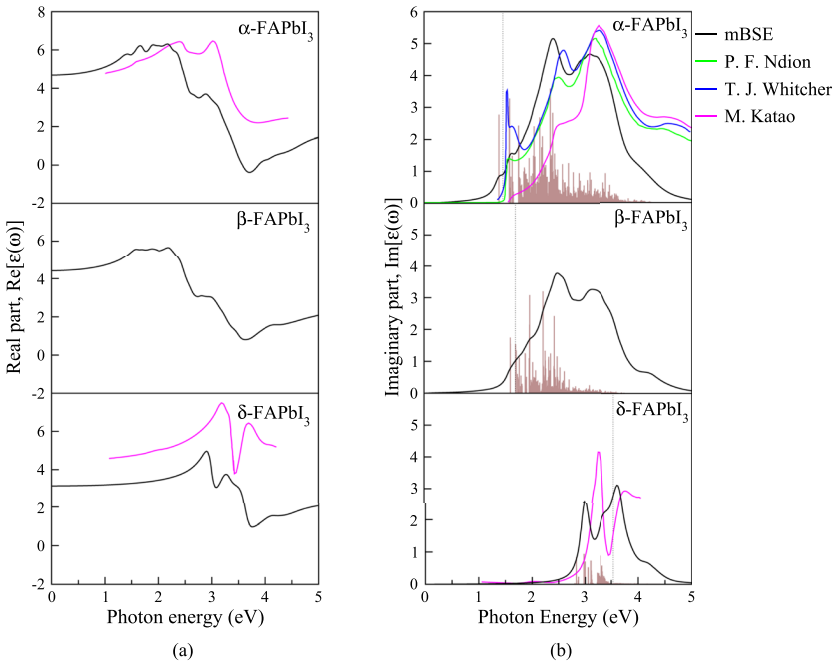

FIG. 4. The mBSE based (a) real ($\mathrm{Re}[\varepsilon(\omega)]$) and (b) imaginary ($\mathrm{Im}[\varepsilon(\omega)]$) parts of dielectric functions with the optical transition oscillator strengths (brown histograms) and G_0W_0 derived electronic bandgap $E_{g(GW)}$ (dashed lines). Note that the real parts are shifted to the converged ε_0 values due to its very slow convergence with respect to the number of orbitals (see the supplementary material for more details). Comparison with the available experimental data is shown for α-$FAPbI_3$ and δ-$FAPbI_3$.[65–67] The data from Ref. 65 are calculated indirectly from the experimentally measured refractive index and extinction coefficient.

TABLE IV. The calculated high frequency dielectric constant ε_∞ and first mBSE eigenvalue Δ^1_{BSE}. The exciton binding energies E_b (meV) are obtained as the difference between $E_{g(GW)}$ and Δ^1_{BSE}.

Phase	ε_∞	Δ^1_{BSE} (eV)	$E_b = E_{g(GW)} - \Delta^1_{BSE}$ (meV)
α-$FAPbI_3$	5.319	1.439	74
β-$FAPbI_3$	4.608	1.595	93
δ-$FAPbI_3$	3.968	2.977	567

to the structural transition of $FAPbI_3$ from the α- to δ-phase. This can be attributed to the dominant intrinsic mechanism of Fröhlich interactions of optically excited charge carriers and longitudinal optical (LO) phonons, resulting in low momentum of charge-carrier with a weak screening environment.[7,68] These optical characteristic is well documented in the experimental studies of phase-dependent emission-line broadening for $MAPbI_3$ and $FAPbI_3$.[69]

Since the structural transition with temperature distorts the PbI_6 framework, which affects the bound state of e–h pair and thus influences the excitonic binding energies, we have deduced the converged exciton binding energies for all the three phases of $FAPbI_3$ using the mBSE approach. We note that the convergence for the exciton binding energies with respect to the k-point mesh is rather slow. As a demonstration of this approach, we show the convergence details for β-$FAPbI_3$ as a representative example in the supplementary material.

The relevant ion clamped dielectric functions ε_∞ (high frequency dielectric constant) are obtained from the G_0W_0+SOC calculations. The calculated exciton binding energies calculated as the difference of G_0W_0 bandgap ($E_{g(GW)}$) and the first bright exciton peak Δ^1_{BSE} are summarized in Table IV. The increasing exciton binding energy with temperature-dependent structural transition is well consistent with decreasing dielectric constant and increasing carrier effective masses. Interestingly, according to Davies *et al.*,[70] the trend in optical bandgap with respect to temperature for the thin film of $FAPbI_3$ is completely opposite as compared to bulk $FAPbI_3$ in the present study. Due to the different morphologies and carrier densities, dissimilar behaviors in carrier mobilities and absorption spectra may be expected for bulk and thin films.[71,72] The first eigenvalue of the BSE solution is calculated to be 1.439 eV for α-$FAPbI_3$, which corresponds to the optical bandgap showing excellent agreement with the experimentally obtained results of 1.43[73] and 1.45 eV.[74] The smaller values of E_b for α-$FAPbI_3$ and β-$FAPbI_3$, in comparison to that for δ-$FAPbI_3$, illustrate large ionic screening and prolonged carrier lifetime at the excited level. Thus, the smaller values of E_b in α-$FAPbI_3$ and β-$FAPbI_3$ require minimum energy for the dissociation of e–h pair, which results in high optical absorption and efficient solar cell performance. Lower rotational entropy in δ-$FAPbI_3$ results in localization of bound excitons and low carrier mobility, thereby increasing E_b. Such results indicate that variation in exciton binding energies is directly related to the rotational entropy of FA molecule as well as the dynamics of the PbI_3 sublattice. This will affect the formation of polarons and active carrier hopping, which can be considered as one of the possible evidences for the long carrier lifetime in $FAPbI_3$.

CONCLUSION

In conclusion, we have studied the relativistic quasi-particle electronic and optical properties of $FAPbI_3$ in their cubic, tetragonal, and hexagonal phases. The computed G_0W_0 bandgap increases from the cubic to hexagonal phases, which is related to the increase in Pb–I bond length in the inorganic framework. From the calculated optical spectra, we find that the spectrum is overall blue shifted from the cubic to hexagonal phases, and the computed optical oscillator strength shows higher values for the cubic and tetragonal phases in comparison to the hexagonal phase. From the mBSE calculations, the exciton binding energies are higher for the hexagonal phase of $FAPbI_3$ than for the cubic and tetragonal phases, indicating their enhanced carrier lifetime and higher light harvesting capabilities. Our results provide useful information on improving efficiencies of the solar cells at different thermal conditions.

SUPPLEMENTARY MATERIAL

See the supplementary material for mBSE optical spectra and exciton binding energy convergence for β-$FAPbI_3$ and ε_0 convergence with respect to number of orbitals for all the three phases of $FAPbI_3$.

ACKNOWLEDGMENTS

Z. Muhammad is thankful to M. Maier for helpful discussions. This work was supported by the Higher Education Commission of Pakistan (HEC) under the Research Project No. 20-3959/NRPU/R & D/HEC2014/234. P. Liu and C. Franchini acknowledge support from the Austrian Science Fund (FWF). Vienna Scientific Cluster (VSC) is gratefully acknowledged for computing facilities.

AUTHOR DECLARATIONS

Conflict of Interest

The authors have no conflicts of interest to disclose.

DATA AVAILABILITY

The data that support the findings of this study are available within the article and its supplementary material.

REFERENCES

[1] Z. Wang, X. Zhu, S. Zuo, M. Chen, C. Zhang, C. Wang, X. Ren, Z. Yang, Z. Liu, X. Xu, Q. Chang, S. Yang, F. Meng, Z. Liu, N. Yuan, J. Ding, S. (Frank) Liu, and D. Yang, Adv. Funct. Mater. **30**, 1908298 (2020).
[2] A. Leblanc, N. Mercier, M. Allain, J. Dittmer, T. Pauporté, V. Fernandez, F. Boucher, M. Kepenekian, and C. Katan, ACS Appl. Mater. Interfaces **11**, 20743 (2019).
[3] K. A. Bush, K. Frohna, R. Prasanna, R. E. Beal, T. Leijtens, S. A. Swifter, and M. D. McGehee, ACS Energy Lett. **3**, 428 (2018).
[4] E. S. Parrott, T. Green, R. L. Milot, M. B. Johnston, H. J. Snaith, and L. M. Herz, Adv. Funct. Mater. **28**, 1802803 (2018).
[5] G. E. Eperon, S. D. Stranks, C. Menelaou, M. B. Johnston, L. M. Herz, and H. J. Snaith, Energy Environ. Sci. **7**, 982 (2014).
[6] J. H. Noh, S. H. Im, J. H. Heo, T. N. Mandal, and S. Il Seok, Nano Lett. **13**, 1764 (2013).

[7]Y. Chen, H. T. Yi, X. Wu, R. Haroldson, Y. N. Gartstein, Y. I. Rodionov, K. S. Tikhonov, A. Zakhidov, X.-Y. Zhu, and V. Podzorov, Nat. Commun. **7**, 12253 (2016).
[8]C. Wehrenfennig, G. E. Eperon, M. B. Johnston, H. J. Snaith, and L. M. Herz, Adv. Mater. **26**, 1584 (2014).
[9]J. Lim, M. T. Hörantner, N. Sakai, J. M. Ball, S. Mahesh, N. K. Noel, Y.-H. Lin, J. B. Patel, D. P. McMeekin, M. B. Johnston, B. Wenger, and H. J. Snaith, Energy Environ. Sci. **12**, 169 (2019).
[10]N. T. P. Hartono, S. Sun, M. C. Gélvez-Rueda, P. J. Pierone, M. P. Erodici, J. Yoo, F. Wei, M. Bawendi, F. C. Grozema, M.-j. Sher, T. Buonassisi, and J.-P. Correa-Baena, J. Mater. Chem. A **7**, 23949 (2019).
[11]G. W. P. Adhyaksa, L. W. Veldhuizen, Y. Kuang, S. Brittman, R. E. I. Schropp, and E. C. Garnett, Chem. Mater. **28**, 5259 (2016).
[12]G. Xing, N. Mathews, S. Sun, S. S. Lim, Y. M. Lam, M. Grätzel, S. Mhaisalkar, and T. C. Sum, Science **342**, 344 (2013).
[13]S. D. Stranks, G. E. Eperon, G. Grancini, C. Menelaou, M. J. P. Alcocer, T. Leijtens, L. M. Herz, A. Petrozza, and H. J. Snaith, Science **342**, 341 (2013).
[14]T. Chen, W.-L. Chen, B. J. Foley, J. Lee, J. P. C. Ruff, J. Y. P. Ko, C. M. Brown, L. W. Harriger, D. Zhang, C. Park, M. Yoon, Y.-M. Chang, J. J. Choi, and S.-H. Lee, Proc. Natl. Acad. Sci. U. S. A. **114**, 7519 (2017).
[15]K. Galkowski, A. Mitioglu, A. Miyata, P. Plochocka, O. Portugall, G. E. Eperon, J. T.-W. Wang, T. Stergiopoulos, S. D. Stranks, H. J. Snaith, and R. J. Nicholas, Energy Environ. Sci. **9**, 962 (2015).
[16]M. Bokdam, T. Sander, A. Stroppa, S. Picozzi, D. D. Sarma, C. Franchini, and G. Kresse, Sci. Rep. **6**, 28618 (2016).
[17]A. Miyata, A. Mitioglu, P. Plochocka, O. Portugall, J. T.-W. Wang, S. D. Stranks, H. J. Snaith, and R. J. Nicholas, Nat. Phys. **11**, 582 (2015).
[18]A. M. Soufiani, F. Huang, P. Reece, R. Sheng, A. Ho-Baillie, and M. A. Green, Appl. Phys. Lett. **107**, 231902 (2015).
[19]Y. Yamada, T. Nakamura, M. Endo, A. Wakamiya, and Y. Kanemitsu, IEEE J. Photovoltaics **5**, 401 (2015).
[20]N. Sestu, M. Cadelano, V. Sarritzu, F. Chen, D. Marongiu, R. Piras, M. Mainas, F. Quochi, M. Saba, A. Mura, and G. Bongiovanni, J. Phys. Chem. Lett. **6**, 4566 (2015).
[21]M. Saba, M. Cadelano, D. Marongiu, F. Chen, V. Sarritzu, N. Sestu, C. Figus, M. Aresti, R. Piras, A. Geddo Lehmann, C. Cannas, A. Musinu, F. Quochi, A. Mura, and G. Bongiovanni, Nat. Commun. **5**, 5049 (2014).
[22]V. D'Innocenzo, G. Grancini, M. J. P. Alcocer, A. R. S. Kandada, S. D. Stranks, M. M. Lee, G. Lanzani, H. J. Snaith, and A. Petrozza, Nat. Commun. **5**, 3586 (2014).
[23]J. M. Frost, K. T. Butler, F. Brivio, C. H. Hendon, M. van Schilfgaarde, and A. Walsh, Nano Lett. **14**, 2584 (2014).
[24]J. M. Frost, K. T. Butler, and A. Walsh, APL Mater. **2**, 081506 (2014).
[25]Y. Kutes, L. Ye, Y. Zhou, S. Pang, B. D. Huey, and N. P. Padture, J. Phys. Chem. Lett. **5**, 3335 (2014).
[26]S. Liu, F. Zheng, N. Z. Koocher, H. Takenaka, F. Wang, and A. M. Rappe, J. Phys. Chem. Lett. **6**, 693 (2015).
[27]T. Etienne, E. Mosconi, and F. De Angelis, J. Phys. Chem. Lett. **7**, 1638 (2016).
[28]E. M. Hutter, M. C. Gélvez-Rueda, A. Osherov, V. Bulović, F. C. Grozema, S. D. Stranks, and T. J. Savenije, Nat. Mater. **16**, 115 (2017).
[29]A. Stroppa, D. Di Sante, P. Barone, M. Bokdam, G. Kresse, C. Franchini, M.-H. Whangbo, and S. Picozzi, Nat. Commun. **5**, 5900 (2014).
[30]F. Zheng, L. Z. Tan, S. Liu, and A. M. Rappe, Nano Lett. **15**, 7794 (2015).
[31]H. Zhu, K. Miyata, Y. Fu, J. Wang, P. P. Joshi, D. Niesner, K. W. Williams, S. Jin, and X. Y. Zhu, Science **353**, 1409 (2016).
[32]C. Franchini, M. Reticcioli, M. Setvin, and U. Diebold, Nat. Rev. Mater. **6**, e1601650 (2021).
[33]X.-Y. Zhu and V. Podzorov, J. Phys. Chem. Lett. **6**, 4758 (2015).
[34]T. Chen, B. J. Foley, C. Park, C. M. Brown, L. W. Harriger, J. Lee, J. Ruff, M. Yoon, J. J. Choi, and S. H. Lee, Sci. Adv. **2**, e1601650 (2016).
[35]M. Shishkin and G. Kresse, Phys. Rev. B: Condens. Matter Mater. Phys. **75**, 235102 (2007).
[36]M. Van Schilfgaarde, T. Kotani, and S. Faleev, Phys. Rev. Lett. **96**, 226402 (2006).
[37]M. R. Filip and F. Giustino, Phys. Rev. B: Condens. Matter Mater. Phys. **90**, 245145 (2014).
[38]M. S. Hybertsen and S. G. Louie, Phys. Rev. Lett. **55**, 1418 (1985).
[39]G. Strinati, H. J. Mattausch, and W. Hanke, Phys. Rev. B **25**, 2867 (1982).
[40]M. L. Tiago and J. R. Chelikowsky, Phys. Rev. B **73**, 205334 (2006).
[41]G. Onida, L. Reining, and A. Rubio, Rev. Mod. Phys. **74**, 601 (2002).
[42]M. Rohlfing and S. G. Louie, Phys. Rev. B **62**, 4927 (2000).
[43]M. T. Weller, O. J. Weber, J. M. Frost, and A. Walsh, J. Phys. Chem. Lett. **6**, 3209 (2015).
[44]V. C. A. Taylor, D. Tiwari, M. Duchi, P. M. Donaldson, I. P. Clark, D. J. Fermin, and T. A. A. Oliver, J. Phys. Chem. Lett. **9**, 895 (2018).
[45]G. Kresse and J. Furthmüller, Phys. Rev. B **54**, 11169 (1996).
[46]G. Kresse and D. Joubert, Phys. Rev. B **59**, 1758 (1999).
[47]P. E. Blöchl, Phys. Rev. B **50**, 17953 (1994).
[48]R. G. Parr, Annu. Rev. Phys. Chem. **34**, 631 (1983).
[49]J. P. Perdew, K. Burke, and M. Ernzerhof, Phys. Rev. Lett. **77**, 3865 (1996).
[50]I. Hamada, Phys. Rev. B **89**, 121103 (2014).
[51]P. Liu, B. Kim, X.-Q. Chen, D. D. Sarma, G. Kresse, and C. Franchini, Phys. Rev. Mater. **2**, 075003 (2018).
[52]P. Liu, C. Franchini, M. Marsman, and G. Kresse, J. Phys.: Condens. Matter **32**, 015502 (2020).
[53]O. J. Weber, D. Ghosh, S. Gaines, P. F. Henry, A. B. Walker, M. S. Islam, and M. T. Weller, Chem. Mater. **30**, 3768 (2018).
[54]B. Slimi, M. Mollar, I. Ben Assaker, A. Kriaa, R. Chtourou, and B. Marí, Monatsh. Chem. **148**, 835 (2017).
[55]Q. Han, S. H. Bae, P. Sun, Y. T. Hsieh, Y. Yang, Y. S. Rim, H. Zhao, Q. Chen, W. Shi, G. Li, and Y. Yang, Adv. Mater. **28**, 2253 (2016).
[56]D. H. Fabini, T. A. Siaw, C. C. Stoumpos, G. Laurita, D. Olds, K. Page, J. G. Hu, M. G. Kanatzidis, S. Han, and R. Seshadri, J. Am. Chem. Soc. **139**, 16875 (2017).
[57]D. H. Fabini, C. C. Stoumpos, G. Laurita, A. Kaltzoglou, A. G. Kontos, P. Falaras, M. G. Kanatzidis, and R. Seshadri, Angew. Chem., Int. Ed. **55**, 15392 (2016).
[58]P. Umari, E. Mosconi, and F. De Angelis, Sci. Rep. **4**, 4467 (2015).
[59]G. Giorgi, J.-I. Fujisawa, H. Segawa, and K. Yamashita, J. Phys. Chem. C **118**, 12176 (2014).
[60]A. Pisanu, C. Ferrara, P. Quadrelli, G. Guizzetti, M. Patrini, C. Milanese, C. Tealdi, and L. Malavasi, J. Phys. Chem. C **121**, 8746 (2017).
[61]W. Gao, X. Gao, T. A. Abtew, Y.-Y. Sun, S. Zhang, and P. Zhang, Phys. Rev. B **93**, 085202 (2016).
[62]E. Menéndez-Proupin, P. Palacios, P. Wahnón, and J. C. Conesa, Phys. Rev. B: Condens. Matter Mater. Phys. **90**, 045207 (2014).
[63]R. Ben Aich, S. Ben Radhia, K. Boujdaria, M. Chamarro, and C. Testelin, J. Phys. Chem. Lett. **11**, 808 (2020).
[64]M. C. Gélvez-Rueda, N. Renaud, and F. C. Grozema, J. Phys. Chem. C **121**, 23392 (2017).
[65]P. F. Ndione, Z. Li, and K. Zhu, J. Mater. Chem. C **4**, 7775 (2016).
[66]T. J. Whitcher, J. X. Zhu, X. Chi, H. Hu, D. Zhao, T. C. Asmara, X. Yu, M. B. H. Breese, A. H. Castro Neto, Y. M. Lam, A. T. S. Wee, E. E. M. Chia, and A. Rusydi, Phys. Rev. X **8**, 021034 (2018).
[67]M. Kato, T. Fujiseki, T. Miyadera, T. Sugita, S. Fujimoto, M. Tamakoshi, M. Chikamatsu, and H. Fujiwara, J. Appl. Phys. **121**, 115501 (2017).
[68]M. Baranowski and P. Plochocka, Adv. Energy Mater. **10**, 1903659 (2020).
[69]A. D. Wright, C. Verdi, R. L. Milot, G. E. Eperon, M. A. Pérez-Osorio, H. J. Snaith, F. Giustino, M. B. Johnston, and L. M. Herz, Nat. Commun. **7**, 11755 (2016).
[70]C. L. Davies, J. Borchert, C. Q. Xia, R. L. Milot, H. Kraus, M. B. Johnston, and L. M. Herz, J. Phys. Chem. Lett. **9**, 4502 (2018).
[71]D. R. Kammler, T. O. Mason, D. L. Young, T. J. Coutts, D. Ko, K. R. Poeppelmeier, and D. L. Williamson, J. Appl. Phys. **90**, 5979 (2001).
[72]M. Ohring, in *Laser-Induced Damage in Optical Materials: 1993, 2114*, edited by H. E. Bennett, L. L. Chase, A. H. Guenther, B. E. Newnam, and M. J. Soileau (SPIE, 1994), p. 624.

[73]S. Pang, H. Hu, J. Zhang, S. Lv, Y. Yu, F. Wei, T. Qin, H. Xu, Z. Liu, and G. Cui, Chem. Mater. **26**, 1485 (2014).
[74]C. C. Stoumpos, C. D. Malliakas, and M. G. Kanatzidis, Inorg. Chem. **52**, 9019 (2013).
[75]M. Senno and S. Tinte, "Mixed Formamidinium-Methylammonium Lead Iodide perovskite from first-principles: Hydrogen-bonding impact on the electronic properties," Phys. Chem. Chem. Phys. **23**(12), 7376–7385 (2021).